ACCURACY OF BACKGROUND ORIENTED SCHLIEREN FOR DIFFERENT BACKGROUND PATTERNS AND MEANS OF REFRACTION INDEX RECONSTRUCTION

N.A. VINNICHENKO[1,c], A.V. UVAROV[1], Yu.Yu. PLAKSINA[1]

[1]Faculty of Physics, Lomonosov Moscow State University, Moscow, 119991, Russia

[c]Corresponding author: Tel.: +74959392741; Fax: +74959328820; Email: nickvinn@yandex.ru

KEYWORDS:

Main subjects: flow visualization, image processing, accuracy analysis
Fluid: thermal boundary layers, evaporation
Visualization method(s): background oriented schlieren
Other keywords: background pattern, synthetic images, blur

ABSTRACT: Different sources of error in Background Oriented Schlieren (BOS) technique for measuring the refraction index field are analyzed. They can be divided into three groups: cross-correlation errors similar to Particle Image Velocimetry (PIV), optical defects of the original images, limiting the capabilities of post-processing, and computational errors associated with procedure of refraction index field reconstruction from its gradient.

The errors of the first group are closely related to the problem of choosing the optimal background pattern. In contrast to PIV, seeding density, size and shape of the pattern elements can be fully controlled to minimize peak-locking and in-plane loss-of-pairs due to limited interrogation window size. In present investigation these errors are estimated for popular multi-pass cross-correlation interrogation with discrete window offset [1] and several types of black-and-white background pattern by generating synthetic images with known displacement field and post-processing them. Constant displacement fields are used to estimate the accuracy and sinusoidal ones — to assess spatial resolution. Best results are shown to be obtained with randomly positioned square dots 2×2 or 3×3 pixels. Also, tests for the displacement gradient error are performed using displacement fields, simulating thermal boundary layers or shock waves.

The errors of the second group include defocusing and distortion of the image elements due to in-plane nonlinear variations of refraction index. Defocusing is simulated by Gaussian blur filter applied to the second image of the pair. Black-and-white square dot patterns, especially ones with larger dots, are shown to be more robust with respect to blur than grayscale wavelet-noise ones.

The third group of errors is specific for BOS. If solving Poisson equation is used, it includes right-hand side error related to displacement evaluation, approximation error of solution due to finite grid step and the error of boundary conditions, estimated from the displacement field. Boundary conditions are shown to add small errors to those of interrogation algorithm. Nevertheless, using smaller interrogation windows (IWs) is required for better spatial resolution of refraction index field.

The results of numerical experiments are proven with real images of thin thermal layers below the surface of evaporating liquids.

Introduction

BOS method, originally proposed by Meier [2], provides quantitative measurements of refraction index, density or temperature fields in gas and liquid flows. The essence of the method is comparison of two images of the same background pattern, taken with and without the investigated transparent object located between the camera and the background. The comparison is usually performed by cross-correlation interrogation, adopted from PIV. It results in displacement field, which is used to reconstruct the density or refraction index field. All the stages of the procedure: optical acquisition of the images, cross-correlation processing and reconstruction of the refraction index field — have certain intrinsic errors which affect the overall accuracy. The goal of the present paper is to model these errors and to

analyze their dependence on different factors being involved like background pattern being used, value of refraction index gradient being measured, cross-correlation strategy and procedure of eventual refraction index field reconstruction. BOS has several distinguishing features in comparison with PIV: 1) pattern distortion originates not from kinematic displacement of particles but from refraction, 2) background pattern is fully controlled, 3) additional computational procedure has to be performed to obtain the resultant refraction index field from the displacement field. Therefore, BOS does not suffer from some of the PIV physical errors like out-of-plane loss-of-pairs or particles which do not follow the flow, but has its own specific one — image blur due to refraction index variations in the investigated flow. Errors, associated with cross-correlation interrogation, are the same encountered in PIV (e.g. peak-locking), but they can be reduced in BOS by proper choice of the background pattern or, possibly, by using interrogation algorithm specially designed for certain type of background. Additional error is introduced by refraction index reconstruction procedure.

The rest of the paper is organized as follows. First, optical errors associated with properties of the investigated object are discussed. This part of the investigation is still under way, hence only problem formulation and some preliminary results are presented. Then, tests for synthetic images with known displacement fields are performed to assess the accuracy of cross-correlation algorithm for various background patterns. Tests include conventional constant and sinusoidal displacement fields for evaluation of accuracy and spatial resolution, as well as special test for influence of displacement gradient, imitating visualization of thin thermal boundary layer or a shock wave. Accuracy of the resultant density (or refraction index) field is analyzed together with accuracy of displacement field, illustrating the influence of the reconstruction procedure. Finally, the results of temperature measurements of evaporating liquids are presented, demonstrating the potential of BOS in real experimental problem, involving thin boundary layer and very small temperature differences.

Optical sources of error

As stated above, BOS suffers neither from out-of-plane loss-of-pairs nor from flow perturbations by the particles. It is essentially non-contact method. However, the refraction index spatial variation, which is measured by BOS, can cause degradation of the distorted image quality and loss of accuracy for displacement evaluation. Assume parallel light rays propagating along z-axis from background pattern through the investigated schlieren object, which has refraction index variation along perpendicular x-axis (Fig. 1a). Rays experience deflection due to refraction, then they are focused by the camera lens (shown by green line) which will be treated here as a thin lens. The result is observed in the focal plane of the lens. Ray paths inside schlieren object, shown in Fig. 1a, are obtained by numerical integration of equations

$$\frac{dx}{ds}=\frac{p_x}{n},\ \frac{dp_x}{ds}=\frac{dn}{dx}$$
$$\frac{dz}{ds}=\frac{p_z}{n},\ \frac{dp_z}{ds}=0. \qquad (1)$$

Refraction index variation is specified as $n(x)=1.33+0.04x+0.2x^2$, imitating typical situation under the surface of evaporating water (see below) with temperature gradient about 500 K/m and significant nonlinearity. Additionally, rays exhibit deflection at the walls of the tank. Glass is supposed flat and thin, and does not introduce extra deflection. All dimensions are given in meters and correspond to shooting small water tank with macrolens. If refraction index varies linearly with x, the deflected rays (shown in red in Fig. 1) are collected at one point, which is displaced with respect to undistorted image focus (undistorted rays are shown in blue). Displacement is about 0.1 mm (~10 pixels if object occupies the entire frame). But if nonlinearity is present, the distorted rays are not focused in the focal plane, resulting in defocused image with radius of blur spot about 0.02 mm (2 pixels). Note that this blur is aligned with direction of displacement gradient. Hence, background pattern elements can be distorted like objects seen in a false mirror. Rays forming the images in the focal plane are shown in Fig. 1b. Of course, blurred image has lower quality and presents a challenge for displacement evaluation algorithm. Thus, objects with highly nonlinear refraction index variations in observation plane like thin thermal layers or shock waves result in image blur and increase of error. Measurements just below the air-water interface suffer also from multiple reflections of light from the interface. Real path of a ray

propagating close to the interface can be very complex and cannot be interpreted as deflection by z -averaged refraction index gradient.

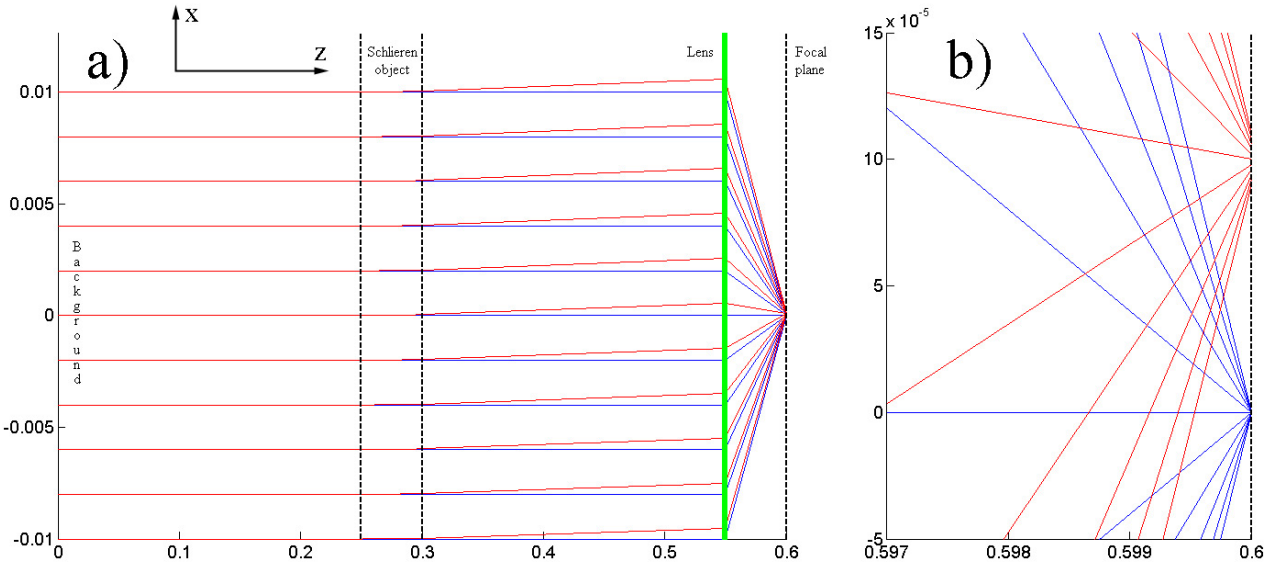

Fig. 1. a) Paths of rays without (blue) and with (red) refraction index variation inside schlieren object. b) Enlarged view of rays forming images in the focal plane.

If point source is considered instead of parallel rays, then certain small blur is observed even for undistorted image due to difference between the air and water refraction indices. Water in tank presents a parallel plate, and even if refraction index is constant, rays are not focused at one point. Obviously, next step is to integrate over point sources located in background plane to obtain image of some kind of background pattern and use it for displacement evaluation tests. This is still to be done. At the moment, image blur is modeled by Gaussian blur digital filter with radius up to 2 pixels.

Cross-correlation interrogation tests

Interrogation algorithm

Displacement field is found by cross-correlation multi-pass interrogation with discrete window offset, close to proposed in [1] and analyzed in [3]. At each pass images are divided into interrogation windows and displacement estimate is found performing trial displacements of each interrogation window in the distorted image. Cross-correlation coefficient is calculated directly, by expression

$$c(a,b) = \frac{1}{N^2} \sum_{i=1}^{N} \sum_{j=1}^{N} \frac{I_1(i,j) - \mu_1}{\sigma_1} \frac{I_2(i+a, j+b) - \mu_2}{\sigma_2}, \qquad (2)$$

where I_1 and I_2 are pixel intensities in reference and distorted images, a and b are trial displacement components, N is IW size, μ_1, μ_2, σ_1 and σ_2 are the means and standard deviations of pixel intensity over IW in each image. IWs are not overlapping. At the next pass each IW is divided into four and integer displacement estimate, obtained at the previous pass, is used as a base for displacement evaluation at smaller IWs. After the final pass sub-pixel displacement values are determined using standard 3-points Gaussian estimator for each direction (see e.g. [4]). No image deformation is used during displacement evaluation. If IW is completely filled with uniform color (in case of small IW and/or background pattern without small details), the correlation coefficient is undefined and the displacement value is replaced by median of valid values from 3×3 stencil. The same is performed if there are two correlation peaks with correlation coefficient difference less than $5 \cdot 10^{-3}$. No further smoothing or outlier rejection was applied to make the accuracy results more clear.

Since the displacement is proportional to refraction index gradient, the refraction index field can be found by solving Poisson equation

$$\frac{\partial^2 n}{\partial x^2}+\frac{\partial^2 n}{\partial y^2}=-\frac{2}{h(2L+h)}\left(\frac{\partial \xi_x}{\partial a}+\frac{\partial \xi_y}{\partial b}\right). \tag{3}$$

Here n is refraction index, ξ is displacement in pixels, h is the object thickness, L is the distance between the background and schlieren object, $a=x/\alpha$ and $b=y/\alpha$ are coordinates in image measured in pixels, α is the size of one pixel of image in background plane (m/pix). Strictly, the problem of n field reconstruction, if its first spatial derivatives $\partial n/\partial x$ and $\partial n/\partial y$ are known, is not equivalent to solving Poisson equation (3). In fact, it is ill-posed because derivatives along two directions are found independently and $\partial^2 n/\partial x\partial y \neq \partial^2 n/\partial y\partial x$. Solving ill-posed problem in terms of minimizing the functional

$$\iint\left(\left(\frac{\partial n}{\partial x}+\frac{2\alpha\xi_x}{h(2L+h)}\right)^2+\left(\frac{\partial n}{\partial y}+\frac{2\alpha\xi_y}{h(2L+h)}\right)^2\right)dx\,dy \tag{4}$$

with help of Euler-Lagrange equations leads to Poisson equation (3). Thus, its solution is regularized solution of the initial ill-posed problem, corresponding to minimum of integral deviation (4).

Note that Eq. (3) requires boundary conditions. One of the boundaries is assumed free from perturbations, undisturbed refraction index value is specified at it. Other boundaries can contain refraction index variation. Natural choice for soft boundary conditions is $\frac{\partial n}{\partial s}=-\frac{2\alpha\xi_s}{h(2L+h)}$, where ξ_s is the displacement component normal to boundary. However, these conditions require accurate values of displacement at the boundary. For tests with synthetic images the nearest displacement value determined by cross-correlation was used but for real images least-squares fit for displacement values from several IWs was applied to avoid noise influence.

In gases density field can be determined afterwards using Gladstone-Dale relation. But in liquids Gladstone-Dale constant depends also on density and temperature. In particular, expanding $\Delta n=G\Delta\rho+\rho\Delta G$ one finds that the second term is about 20-25% of the first one. Hence, density and temperature are found by solving the system of two algebraic equations — empirical equation of state and Lorentz-Lorenz formula for refraction index — at each IW. This is described in more detail in [5]. For synthetic images tests "gas" formulation is used and density field accuracy is analyzed.

Background patterns and synthetic images generation

Small (200×200) fragments of all types of backgrounds being tested are shown in Fig. 2. Chaotic background is composed of randomly positioned black squares with side l. They are allowed to touch but intersections are forbidden in order to keep constant the detail size. Total area fraction covered by squares (source density) is p, which yields average number pN^2/l^2 of squares inside IW (image density). Note that image density is highly uniform, which is so hard to reach in PIV. Opposite to PIV, black squares and white background are considered only because they are more easy to print. Regular background is composed of similar squares with white spaces of length d between them. The source density is $l^2/(l+d)^2$ and IW contains $N^2/(l+d)^2$ squares. Wavelet-noise background was proposed in [6]. It is constructed by summing over different k the differences between $2^k\times 2^k$ random noise images and their downsampled (by factor of 2) versions. Since each of the terms contains elements of definite size (i.e. random noise in a narrow frequency band), the background has details of any spatial scale, which makes it possibly universal for the use in BOS regardless of IW size and displacement value. Besides, it is a grayscale image with continuous histogram, not black-and-white as the patterns composed of black squares. Besides the original pattern (Fig. 2c), a version with enhanced contrast was prepared by setting the mean intensity 127 and standard deviation 77 (Fig. 2d). Surprisingly, no significant difference in performance was found during the tests. Perhaps, global contrast is important only in real experiment

when lens quality is involved. Background patterns, composed of lines, are also used by some authors [7]. However, they require special interrogation algorithm since they are invariant to displacements along the lines. Thus, they cannot be used to determine two-component displacement field. All the patterns are generated by specially designed computer codes. 8-bit 2048×2048 images are recorded as low-compression jpg files.

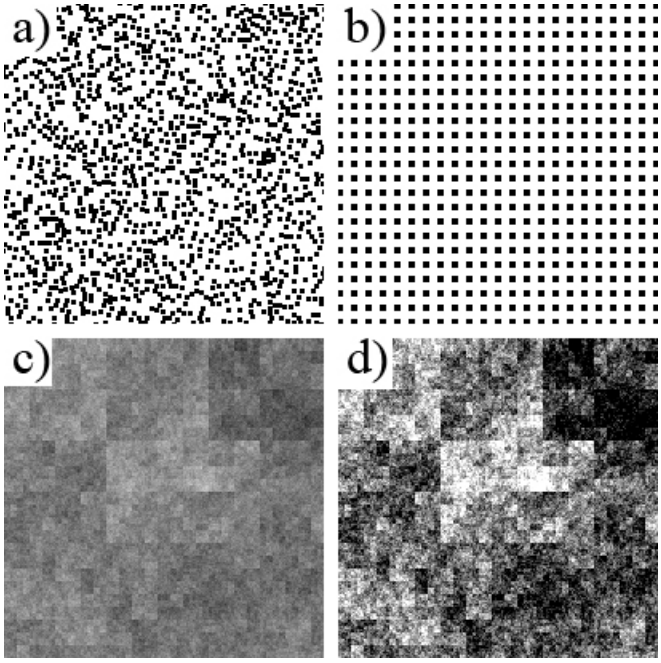

Fig. 2. Background patterns: a) chaotic, b) regular, c) wavelet-noise, d) wavelet-noise with enhanced contrast.

In PIV a synthetic image is composed of individual particle images with known positions. Therefore, the displaced image is obtained by adding the displacement to each particle position and recalculating pixel intensities. However, in BOS the image is just any grayscale image. In order to obtain a distorted image with non-integer displacement pixel intensities have to be recalculated using one of interpolation schemes as done in image deformation techniques. In the present study bilinear interpolation was used. After computing the distorted image, the images are cropped, only the central part 1024×1024 is left for interrogation analysis. All parameters of the optical setup required for density field reconstruction are taken typical for small-scale BOS experiment. Gladstone-Dale constant for air $2.26 \cdot 10^{-4}$ m^3/kg is used and density at the left border is set to 1 kg/m^3. Interrogation is performed with one to four passes, beginning with 32×32 IW.

Constant displacement tests

Accuracy of displacement evaluation is assessed by constant displacement tests, conventional for PIV. The prescribed displacement field is $\xi_x = u = const, \xi_y = 0$. Horizontal displacement value is varied from 0 to 2 pix with step 0.1 pix. Accuracy of displacement evaluation is estimated in terms of bias and random errors for the displacement $\beta_\xi = <\xi_x> - u$, $\sigma_\xi = \sqrt{<(\xi_x - <\xi_x>)^2>}$, with total error given by $\delta_\xi = \sqrt{\beta_\xi^2 + \sigma_\xi^2} = \sqrt{<(\xi_x - u)^2>}$. Density field reconstruction errors are: bias error $\beta_\rho = <\rho - \rho_{exact}>$, random error $\sigma_\rho = \sqrt{<(\rho - \rho_{exact} - \beta_\rho)^2>}$ and total error $\delta_\rho = \sqrt{\beta_\rho^2 + \sigma_\rho^2} = \sqrt{<(\rho - \rho_{exact})^2>}$, where ρ_{exact} is exact solution, determined using the density-displacement relation and prescribed displacement field.

Well-known peak-locking effect is illustrated in Fig. 3 by plotting the displacement bias error. As in PIV, bias error is high for the pattern with element size of 1 pixel and is less than 0.1 pix for the rest. Wavelet-noise background exhibits slightly stronger peak-locking than chaotic dot patterns.

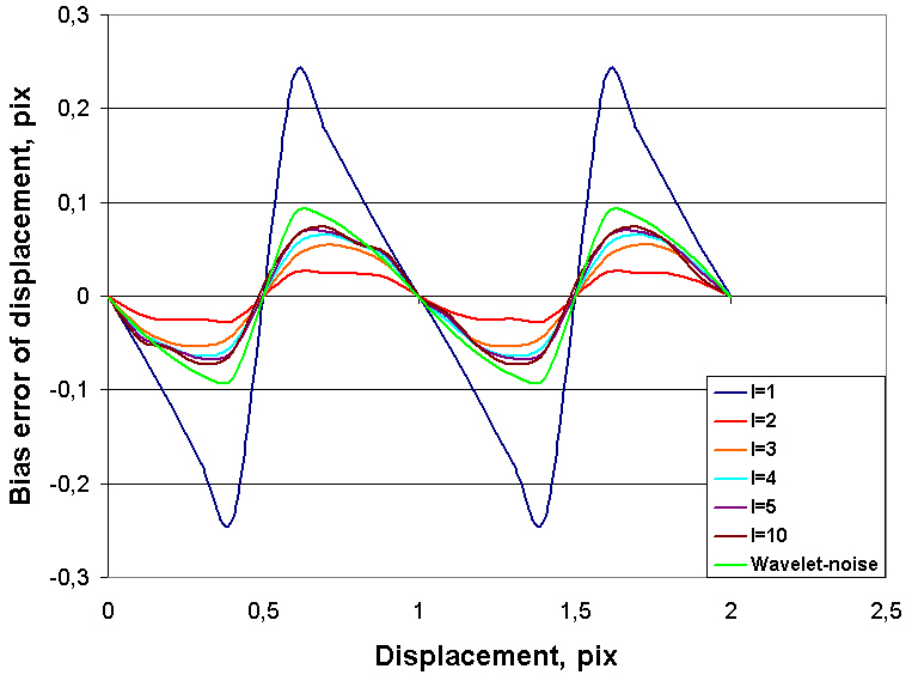

Fig. 3. Bias error of displacement as function of the imposed constant displacement for chaotic backgrounds with p=0.3 and different l, and for wavelet-noise background. 3 interrogation passes are performed in each case.

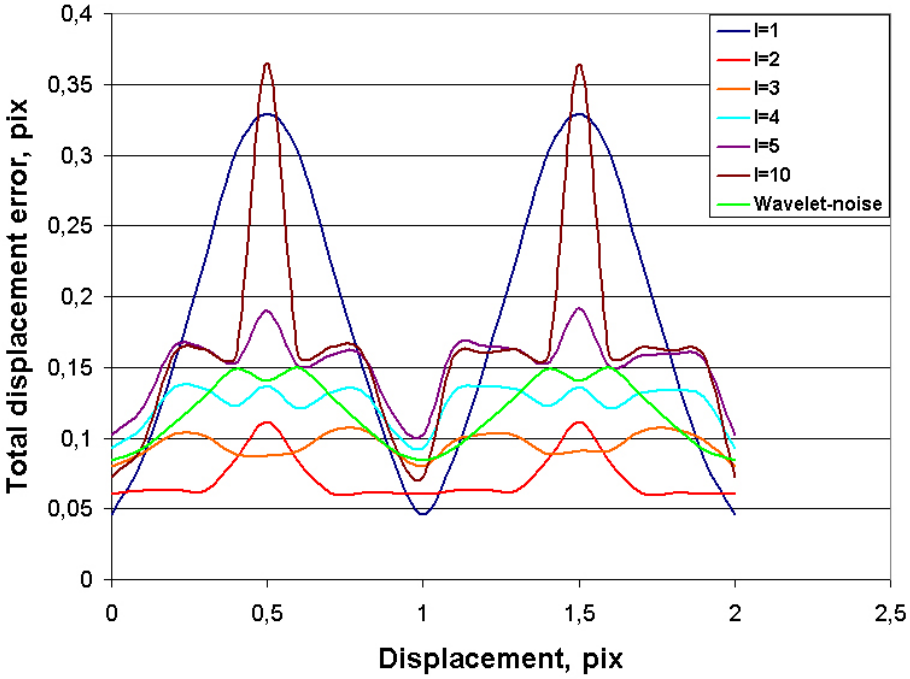

Fig. 4. Total displacement error as function of the imposed displacement for chaotic backgrounds with p=0.3 and different l, and for wavelet-noise background. 3 interrogation passes are performed in all cases.

Influence of the pattern detail size on total displacement error is illustrated in Fig. 4. The best performance is achieved with chaotic backgrounds with $l = 2$ or 3. For larger dots the average number of dots inside the initial IW is not sufficient (for $l = 5$ it is about 12), which leads to accuracy loss by increase of random error. Wavelet-noise background yields moderate results with total error more than 0.1 pix.

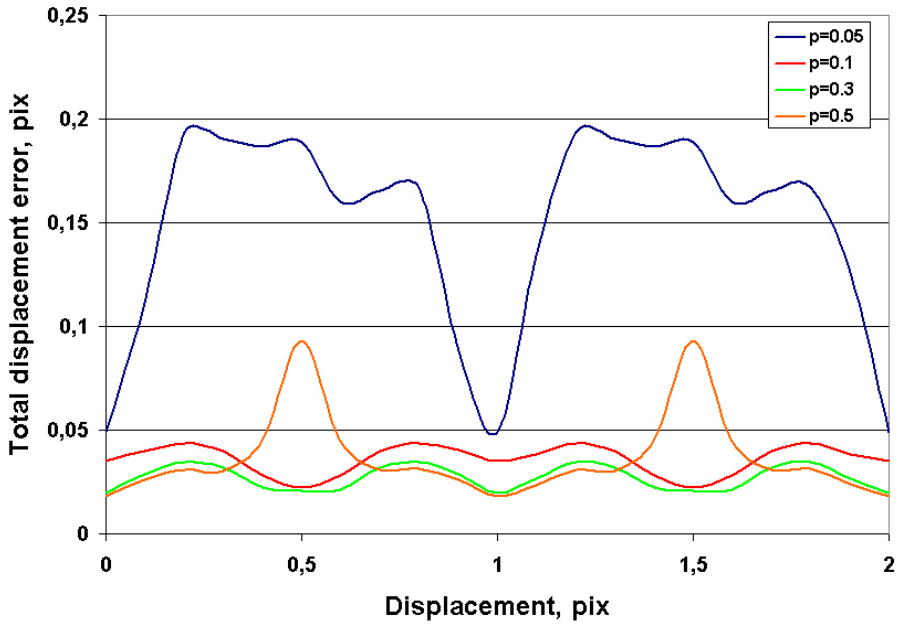

Fig. 5. Total displacement error as function of the imposed displacement for chaotic backgrounds with l=2 and various values of source density p. 2 interrogation passes are performed in all cases.

Source density of the background pattern has minor influence on the error, at least if image density at the final pass is sufficient. Fig. 5 shows that error is significantly increased only for very low source density $p = 0.05$, for which the final IW contains only 3.2 dots.

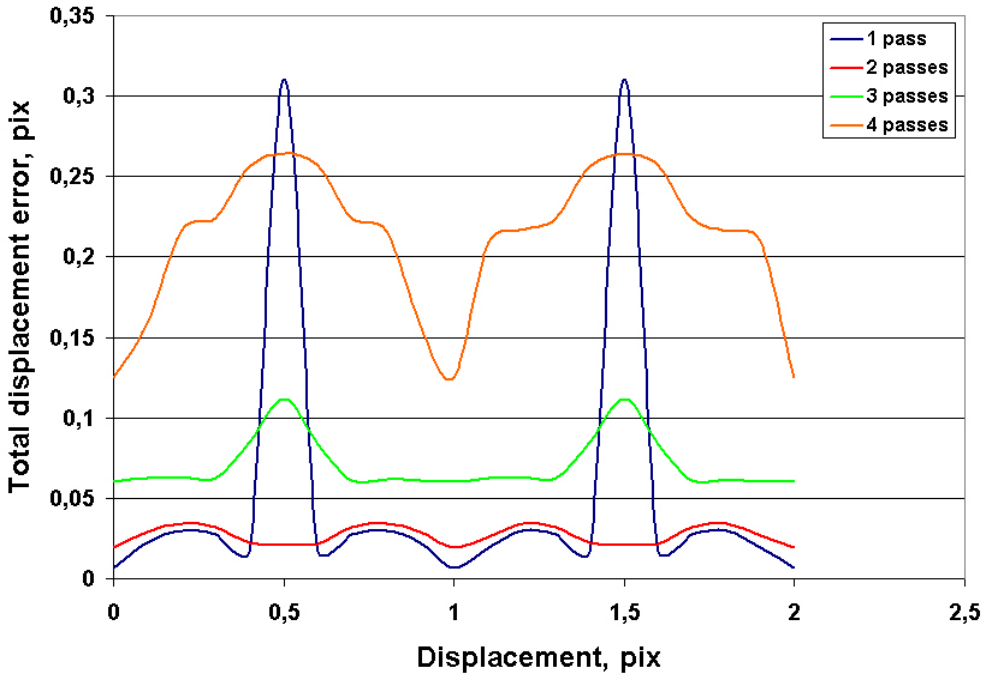

Fig. 6. Total displacement error as function of the imposed displacement for chaotic background with l=2 and p=0.3.

Typical behavior of the displacement error with respect to number of interrogation passes is shown in Fig. 6. The error is minimal for 2 passes. Further reduction of IW size leads to insufficient image density (for the case shown in Fig. 6 it is 19.2 for 2 passes and 4.8 for 3 passes) and loss of accuracy. Obvious exceptions are background with 1-pixel dots, for which bias error due to peak-locking is dominating irrespective from number of passes, and backgrounds with very low

source density, for which image density is insufficient even at the second pass. For wavelet-noise pattern the error for 2 passes is almost the same as for 1 pass.

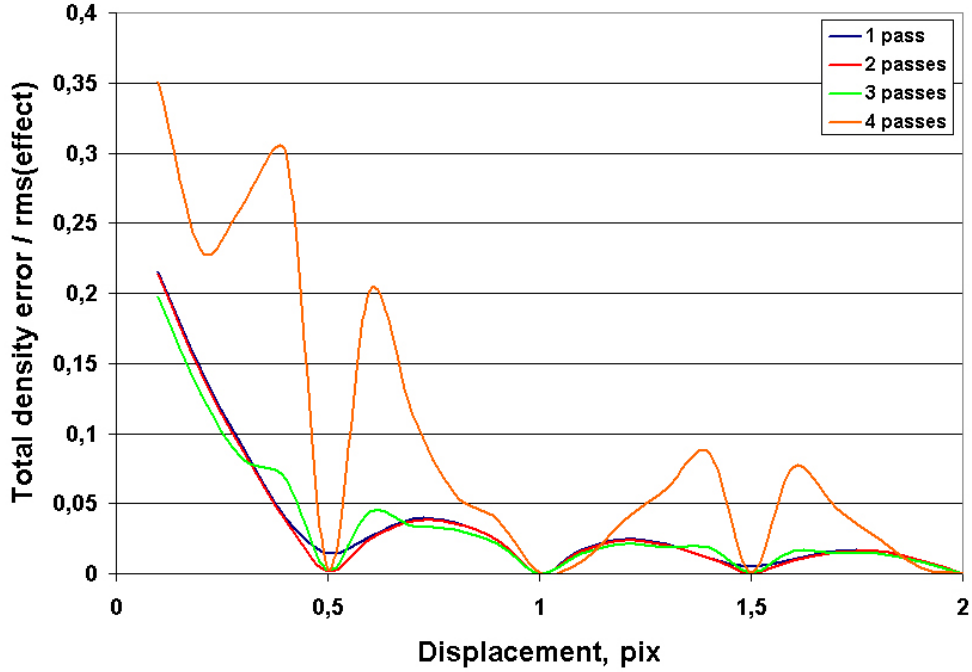

Fig. 7. Total error of density, normalized by rms density change, for chaotic background with l=2 and p=0.3.

The situation is different for density. Fig. 7 shows total density error, normalized by root-mean-square of the density change $\sqrt{<(\rho_{exact}-\rho_0)^2>}$ for the same background as Fig. 6. Though the displacement error is increased at the third interrogation pass, density measurements have almost the same accuracy with 1, 2 and 3 passes. The reason is that Poisson equation solution is solved using more detailed mesh, and approximation error is reduced. The fourth pass, however, worsens the performance because of low image density. Two types of boundary conditions for Poisson equation were tested: boundary conditions with displacement values, taken from exact solution, and boundary conditions with displacement values, evaluated by cross-correlation interrogation. The result is that error in boundary conditions increases total error, but insignificantly. Generally, the accuracy about 2-3% can be achieved for displacements more than 1 pix.

Regular backgrounds show similar behavior, but have certain disadvantages. They are invariant to translations for their period $l+d$. If the maximal displacement, which is tried during interrogation procedure (e.g. half of IW size N) is larger or equal to the background period, two identical correlation peaks emerge and interrogation fails. The requirement $N/2<l+d$ makes image density $N^2/(l+d)^2$ be less than 4, which is insufficient for accurate interrogation. This can be overcome by using large IWs with severe restrictions for maximal displacement (e.g. limiting by $N/4$ leads to image density 16, which is acceptable). This is not convenient and regular patterns can be recommended only if chaotic ones are unavailable as in studies of small water drops, where diffraction gratings are the only available patterns to be used in BOS.

Sinusoidal displacement tests

The displacement field for spatial resolution estimate is prescribed as $\xi_x = 2\sin(2\pi x/\lambda), \xi_y = 0$, where λ is wavelength, and both x and λ are measured in pixels. The same formulation was used in [8] for PIV. Wavelength value is varied from 20 to 150 pix with step 5 pix. Accuracy is characterized by total displacement error $\delta_\xi = \sqrt{<(\xi_x-\xi_{exact})^2>}$, normalized by $\sqrt{<\xi_{exact}^2>}$, and total density error $\delta_\rho = \sqrt{<(\rho-\rho_{exact})^2>}$, normalized by $\sqrt{<(\rho_{exact}-\rho_0)^2>}$. The results for the displacement are given in Fig. 8. Spatial resolution appears to depend on

interrogation procedure rather than background pattern. The second and the third passes enhance it greatly, reaching normalized total error 0.5 at $\lambda \approx 25$-30 pix. Error curves for 1-pass interrogation exhibit strong modulation at wavelengths multiple of IW size. The fourth pass increases the error as in case of constant displacement field. Total density error follows the same trends with normalized total error 0.5 reached at $\lambda \approx 30$-35 pix with 3 interrogation passes.

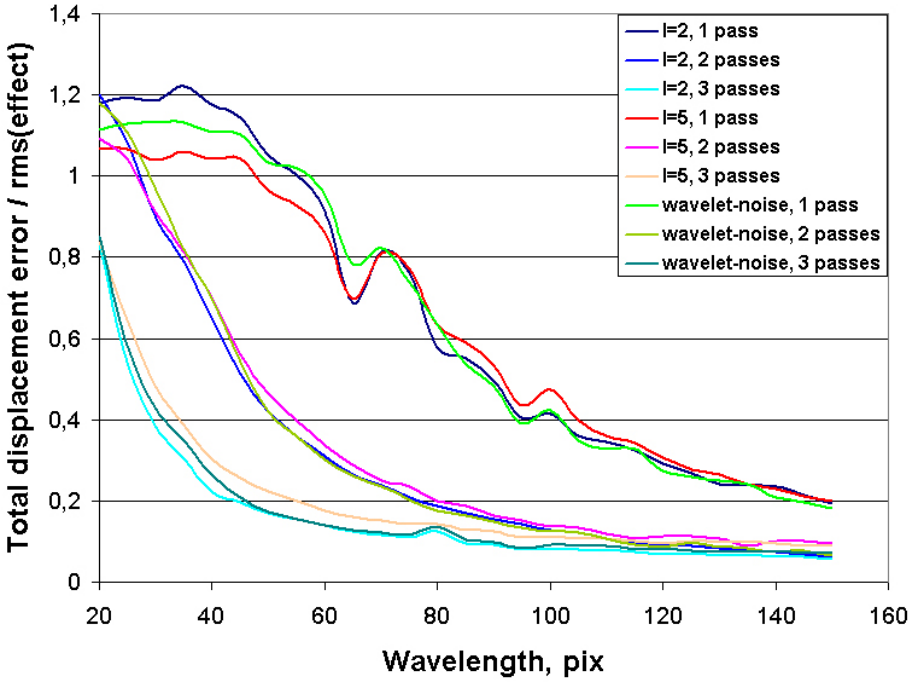

Fig. 8. Spatial resolution test for chaotic backgrounds with l=2, 5 and p=0.3 and wavelet-noise background. The results are given for different number of interrogation passes.

Displacement gradient tests

One of the sources of error in PIV is velocity gradient, which deforms the particle image patterns leading to possible break-up of the correlation peak [4, 9]. The error is known to increase for large IW, yet no commonly-accepted test was elaborated. The same problem is encountered in BOS if the displacement gradient (i.e. second spatial derivative of refraction index) is large. Thin thermal layers and shock waves are typical examples. Usually, high values of displacement gradient are accompanied by high values of displacement, which excludes usage of small IWs in such areas — trick, employed in PIV of boundary layers. The displacement field prescribed for the tests was imitating flat thermal layer: $\xi_y = 0$, $\xi_x(x)$ decreasing linearly from zero at the boundary to $-A$ with increment b and increasing back to zero (Fig. 9a). Primary goal is to investigate the displacement gradient influence, not that of boundary conditions, so the displacement is zero at the boundaries. The width of perturbed region and total density variation depend on b, hence the comparison is made on the base of total errors, normalized by rms of the effect, and the accuracy of total density jump reproduction. For high values of the displacement gradient b interrogation algorithm fails to reproduce maximal (in absolute value) displacement. This results in underestimation of density jump (Fig. 9b), which is generally observed in BOS measurements of flows involving shock waves [10]. The shock wave position is measured with accuracy of BOS spatial resolution (i.e. about 30 pix) and density distribution inside the front is not reproduced. However, reproduction of the total variation is absolutely necessary for the entire density field to be adequate.

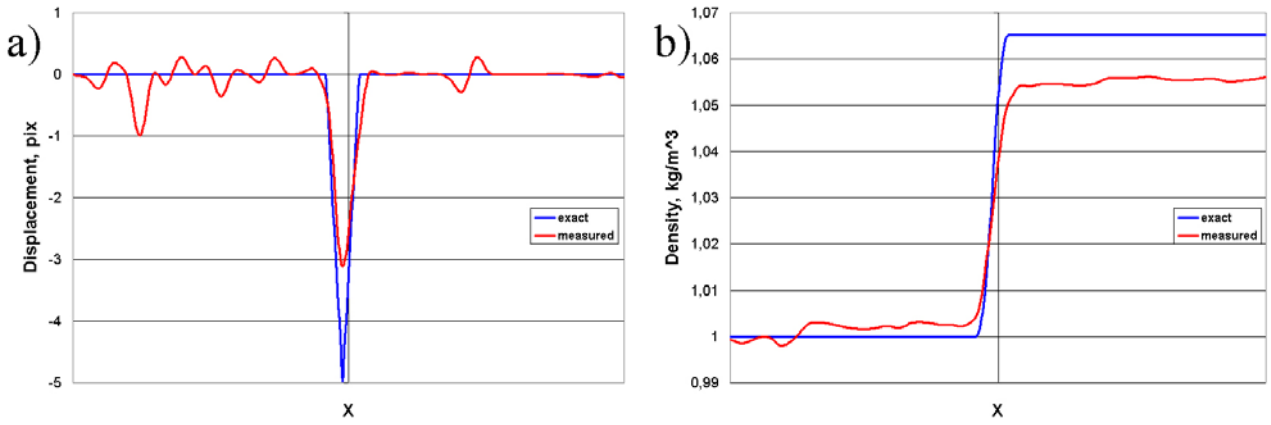

Fig. 9. An example of measurement failure at high displacement gradient value. Profiles of a) displacement, b) density.

Displacement amplitude A was taken equal 5 pix, which corresponds to typical experimental conditions. As in the case of spatial resolution tests, simulation results show that accurate reproduction of the density jump depends rather on number of interrogation passes than on the background pattern (Fig. 10). With 2 or 3 passes density jump is well captured up to displacement gradient 0.3 pix/pix, which is surprisingly high value. Note that the width of the entire transition area for this gradient value is only 34 pix (2 IWs at second pass or 4 IWs at the third one), approaching spatial resolution limit. Good agreement is kept even with four passes, despite total displacement error is high in this case.

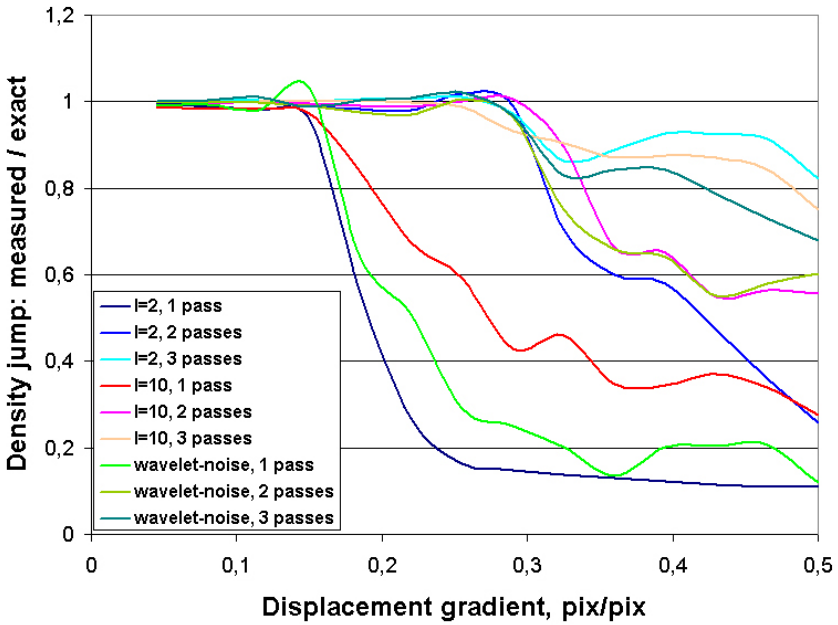

Fig. 10. Total density jump reproduction by chaotic backgrounds with l=2, 10 and p=0.3 and wavelet-noise background. The results are given for different number of interrogation passes.

Image blur effect

As stated above, nonlinear variation of refraction index gradient in observation plane can lead to significant defocusing and blur of the distorted image. This effect can be imitated by blurring uniformly the entire distorted image with Gaussian blur filter of certain radius. Though this imitation does not reproduce all features of the real phenomenon (really, only areas with high nonlinearity of refraction index distribution are blurred and blur is aligned with displacement gradient direction), it gives a rough estimate of blur influence on accuracy of cross-correlation interrogation. All the tests described above were repeated taking into account blur of the second image in each pair (the distorted one) with blur filter radius BFR=0.5, 1, 1.5 and 2 pix. The first image of the pair (the reference one) was not exposed to blur as it is merely a background image taken without refraction index variation in the flow. The results of

constant displacement test, presented in Fig. 11, show that wavelet-noise pattern is much more vulnerable with respect to blur than the backgrounds, composed of randomly positioned squares. When blur filter radius increases, the random error becomes dominant over the bias error due to peak-locking. The total error dependence on the displacement value becomes weak. For BFR=1.5 the total error for wavelet-noise pattern is four times larger than for the optimal background composed of squares with $l = 2$. The same is true for other patterns composed of square dots: at BFR=0.5 the pattern with $l = 4$ yields larger error than wavelet-noise one, but at BFR=1 the error for wavelet-noise pattern is even larger than for $l = 4$ at BFR=1.5. Small amount of blur can even enhance the performance of pattern with $l = 1$ increasing the effective size of dots and decreasing the peak-locking error.

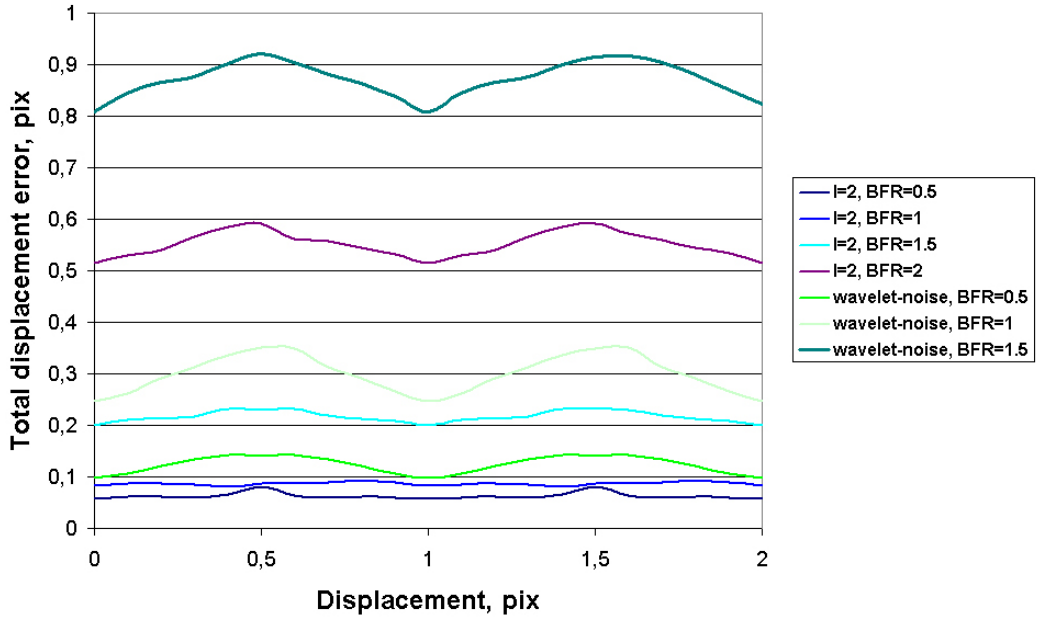

Fig. 11. Influence of blur on accuracy of constant displacement measurements using chaotic background with l=2 and p=0.3 and wavelet-noise background. 3 interrogation passes are performed in all cases.

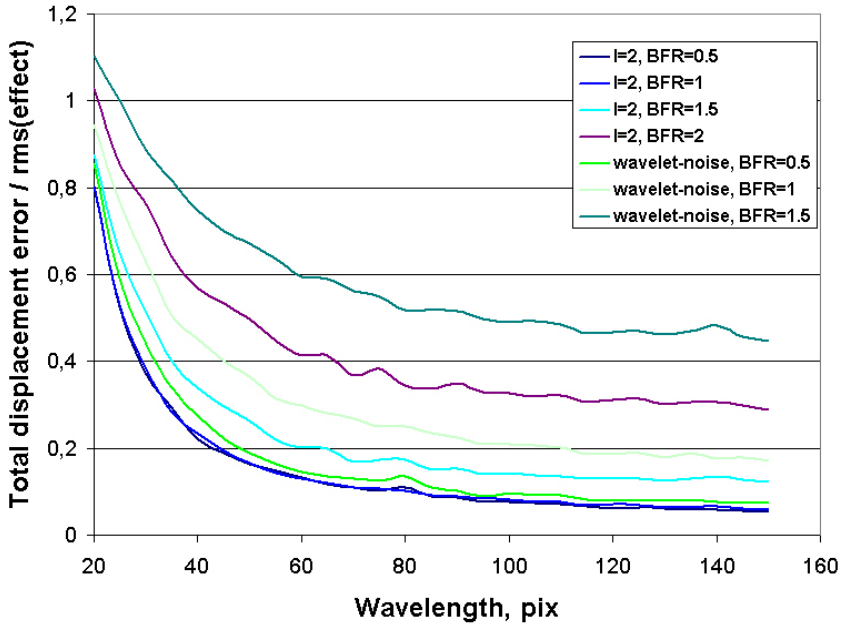

Fig. 12. Influence of blur on spatial resolution for chaotic background with l=2 and p=0.3 and wavelet-noise background. 3 interrogation passes are performed in all cases.

Spatial resolution reached in sinusoidal displacement test declines with blur radius increase: for pattern with $l = 2$ it is 25 pix (with total error 0.5) for BFR=0.5 or 1, 30 pix for BFR=1.5 and only 50 pix for BFR=2. Wavelet-noise pattern performance degrades much more quick: 25-30 pix for BFR=0.5, 35 pix for BFR=1 and 95 pix for BFR=1.5. All the tested wavelengths are not resolved with BFR=2. It is interesting that patterns with larger dots are less vulnerable to blur. At BFR=2 the pattern with $l = 5$ performs better than the pattern with $l = 2$.

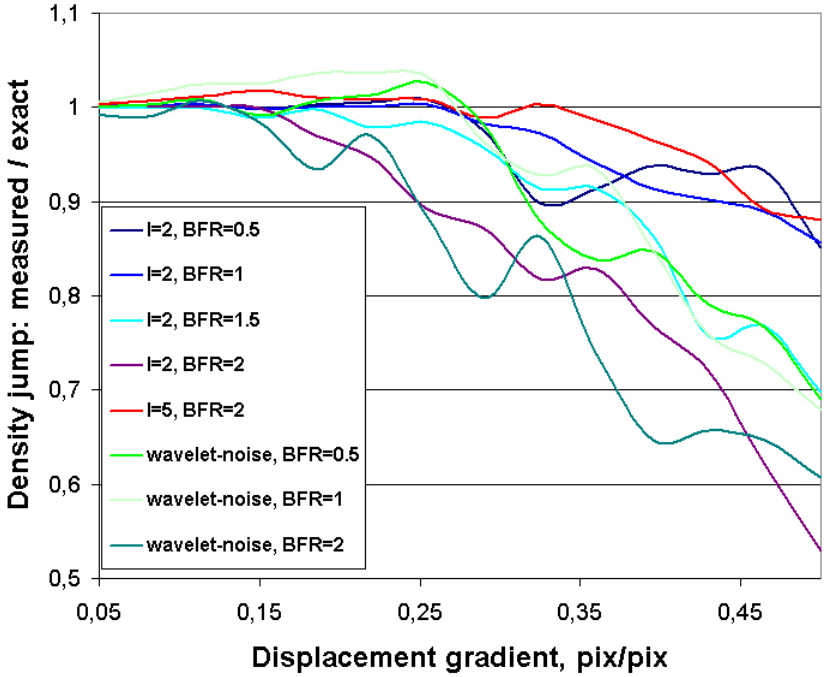

Fig. 13. Influence of blur on accuracy of density jump reproduction for chaotic backgrounds with l=2, 5 and p=0.3 and wavelet-noise background. 3 interrogation passes are performed in all cases.

Background pattern with $l = 2$ reproduces the density jump well up to BFR=1 and degrades for more intense blur (Fig. 13). Wavelet-noise pattern degrades even earlier. The pattern with $l = 5$ yields good measurements of the density jump irrespective from blur intensity.

Real images: cooling below the surface of evaporating liquid

Experimental verification of BOS method accuracy and spatial resolution was performed by measuring temperature fields of evaporating liquids simultaneously by BOS (in vertical plane i.e. side view) and FLIR SC7000 IR thermal imaging device (surface temperature). The surface of liquid is cooled by evaporation. Also, in case if bulk temperature of liquid exceeds room air temperature, liquid is cooled through the tank walls. This problem presents serious experimental challenge because temperature variations are very small (about 0.1 K) and the cool layer near the surface is very thin (about 1 mm). Evaporation proceeds non-uniformly along the liquid surface and under certain conditions this layer can contain small structures, formed by Marangoni convection. This imposes extra requirements for spatial resolution of experimental method. Another issue is the vicinity of liquid-air interface which reflects light, making measurements by optical methods difficult. On the other hand, the flow is nearly 2D, which allows flat BOS implementation without tomographical reconstruction of 3D field.

BOS images were taken with Canon EOS 550D digital SLR camera with kit zoom lens 18-55 mm in 55 mm position. The distance from lens to small tank (50×30×18 mm) with liquid was about 30-40 cm, from the tank to the background about 1.5 m. The camera and the tank were aligned so that liquid surface was located exactly in the middle of the frame in order to minimize light reflections from the surface. Background pattern composed of randomly distributed square dots was used. The size of individual dot image was about 2-3 pix. The background was illuminated by electric lamps.

Exposure time was 1/20 s for aperture f/14 at ISO 800. Reference image was taken closing the tank with cover, thereby ceasing evaporation. Then the cover was removed and the distorted image taken. Significant blur was observed near the liquid surface in the distorted image due to refraction index gradient. Images were cropped below the liquid surface to avoid errors associated with complex ray paths near the interface. Cropped image size was about 1500×800 pix. Images were interrogated with 3 passes, beginning from IW size 20 pix. Maximal displacements observed for the tank thickness 1.8 cm were about 5 pix for water and 10 pix for ethanol which has larger dn/dT . Global displacement, which can be produced while opening the cover, was averaged over the lower part of the flowfield, where no physical effect is expected, and subtracted from the calculated displacement field. Normalized median outlier rejection [11] was additionally performed to suppress noise before solving Poisson equation for refraction index.

Temperature fields obtained by BOS for warm water and room-temperature ethanol are presented in Figs. 14a and 15a respectively. Thermal imaging measurements were averaged over the BOS line-of-sight to make possible the comparison of surface temperature horizontal distributions. Thermal imaging measures temperature averaged over the layer about 0.1 mm below the surface due to intense absorption of IR radiation in liquids. In contrast, BOS experiences difficulties in resolving temperature distribution in layer adjacent to the interface. Both thermal imaging and BOS were calibrated using thermocouple measuring bulk liquid temperature. However, the accuracy of thermocouple is 0.1 K only, which is comparable with temperature variations measured by both methods. Hence, the agreement of absolute temperature values measured by these two methods can be somewhat arbitrary. Nevertheless, correlation of horizontal distributions shown in Figs. 14b and 15b is obvious. Cold liquid layer of 1 mm (38 pix) depth is adequately resolved by BOS. Average temperature gradient at water surface, evaluated by BOS, is 150 K/m, which is remarkably low in comparison with 500 K/m — value obtained from thermophysical experiments. This results from the fact that temperature gradient is maximal just below the surface, and this region is not resolved by BOS or, presumably, can be lost when cropping the images.

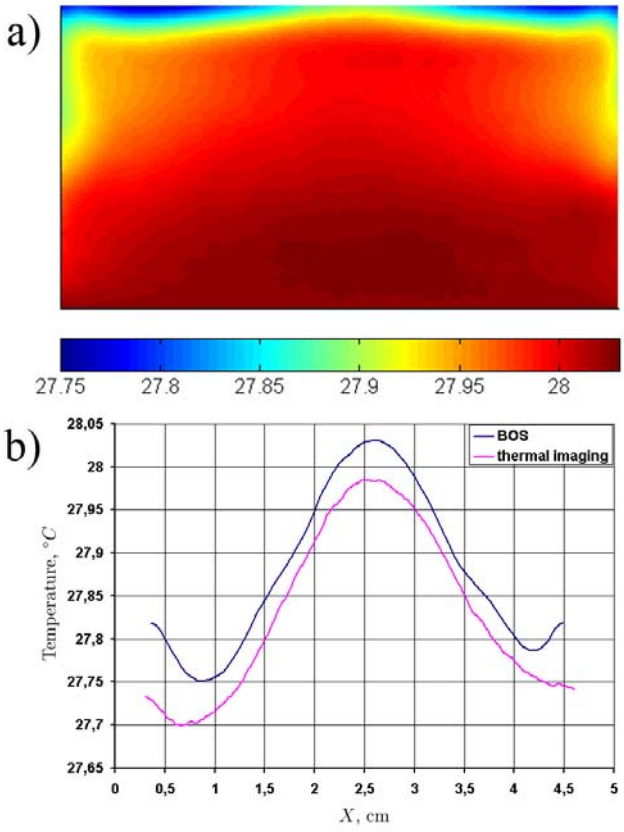

Fig. 14. Temperature measurements in water. a) BOS temperature field (°C), b) comparison of profiles obtained by BOS and thermal imaging. Bulk water temperature is 28.3°C, air temperature is 23.6°C.

Measurements in ethanol show presence of Marangoni convection filaments of cold liquid with typical wavelength about 5 mm which is confirmed by thermal imaging.

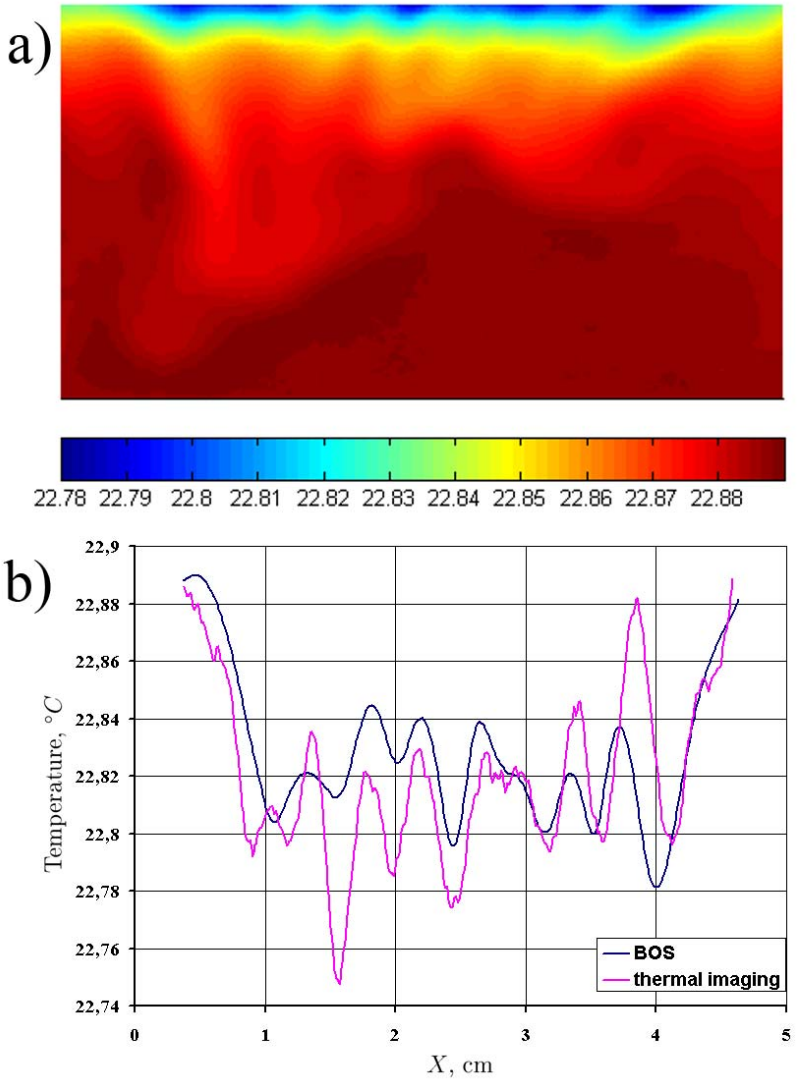

Fig. 15. Temperature measurements in ethanol. a) BOS temperature field (°C), b) comparison of profiles obtained by BOS and thermal imaging.

Conclusions

Various sources of errors for BOS measurements of refraction index, density or temperature have been analyzed: optical loss of image quality, errors of cross-correlation algorithm similar to PIV, errors of refraction index (or density) reconstruction from its first spatial derivatives. In contrast to PIV, reference image (the background pattern) is fully controlled in BOS, which helps to minimize the errors. According to accuracy tests with constant displacement field, best results are obtained with patterns composed of randomly distributed dots with size 2 or 3 pix. Smaller dots result in peak-locking whereas larger ones lead to increase of displacement random error. One should perform as many passes of multi-pass interrogation algorithm as possible assuming that image density exceeds 7-10 “particles” inside IW, as recommended in PIV. Patterns with high source density (e.g. 0.3) should be preferred because they allow using smaller IWs (more interrogation passes). Accuracy about 2-3% of total variation can be achieved for density field if the displacement is more than 1 pix. Increasing the number of interrogation passes has little influence on the accuracy of density field (unlike the displacement field), but enhances spatial resolution and capability to reproduce total variation

of density in flows with displacement gradient (i.e. second spatial derivative of density). Generally, spatial resolution about 25-30 pix and robustness up to displacement gradient 0.3 pix/pix can be achieved with current image processing algorithm. For larger displacement gradients density jump is underestimated in thin structures like thermal boundary layers or shock waves. Boundary conditions for Poisson equation are shown to produce small errors compared to overall performance of interrogation algorithm. Accuracy, spatial resolution and robustness with respect to displacement gradient are worsened for blur, which can be produced by nonlinear variations of refraction index. All characteristics are significantly decreased for blur corresponding to filter radius 2 pix. Wavelet-noise pattern, proposed in [6], yields moderate accuracy but is very vulnerable with respect to blur. Hence, it can be recommended only if no significant image blur is observed and there is no opportunity (or will) to adapt the background pattern so that the dot image size is 2-3 pix. In contrast, patterns with large dot size (~5 pix) are very robust with respect to blur and under heavy blur can outperform "optimal" pattern with 2-pix dots. Regular dot patterns have serious limitations because they are invariant to translations for their period. They should be used only if irregular pattern is unavailable. Large IWs with severe limitations on maximal displacement (like one-quarter rule in PIV) have to be used with such patterns. Good accuracy and spatial resolution of BOS measurements have been confirmed for real test case of temperature fields under the surface of evaporating liquids. Temperature variations as small as 0.1 K can be reliably measured and boundary layers as thin as 1 mm can be resolved. These results are confirmed by simultaneous measurements of surface temperature using IR thermal imaging.

Acknowledgement

This work was partially supported by Russian Foundation of Basic Research (grant 12-08-01077-a).

References

1. Scarano F. and Riethmuller M.L. *Iterative Multigrid Approach in PIV Image Processing with Discrete Window Offset*. Exp. Fluids. 1999, **26** (6), p. 513
2. Meier G.E.A. *Hintergrund-Schlierenverfahren.* Deutsche Patentanmeldung DE 199 42 856 A1, 1999.
3. Westerweel J., Dabiri D. and Gharib M. *The effect of a discrete window offset on the accuracy of cross-correlation analysis of digital PIV recordings*. Exp. Fluids. 1997, **23** (1), p. 20
4. Raffel M., Willert C.E., Wereley S.T. and Kompenhans J. *Particle Image Velocimetry*. Springer, Berlin, 2007
5. Znamenskaya I.A., Vinnichenko N.A. and Glazyrin F.N. *Application of Background Oriented Schlieren method to the studies of flows of non-isothernal fluid*. *Proc. of PSFVIP-8*, Moscow, Russia, 2011.
6. Atcheson B., Heidrich W. and Ihrke I. *An evaluation of optical flow algorithms for background oriented schlieren imaging*. Exp. Fluids. 2009, **46** (3), p. 467
7. Dalziel S.B., Hughes G.O. and Sutherland B.R. *Whole-field density measurements by 'synthetic schlieren'*. Exp. Fluids. 2000, **28** (4), p. 322
8. Nogueira J., Lecuona A. and Rodríguez P.A. *Local field correction PIV: on the increase of accuracy of digital PIV systems*. Exp. Fluids. 1999, **27** (2), p.107
9. Huang H.T., Fiedler H.E. and Wang J.J. *Limitation and improvement of PIV. Part I: Limitation of conventional techniques due to deformation of particle image patterns.* Exp. Fluids. 1993, **15** (3), p. 168
10. Jin. J et al. *Application of BOS method for analysis of the flow after surface discharge. Proc. of ISTP-21*, Kaohsiung, Taiwan ROC, 2010.
11. Westerweel J. and Scarano F. *Universal outlier detection for PIV data*. Exp. Fluids. 2005, **39** (6), p.1096